





# RBFleX-NAS: Training-Free Neural Architecture Search Using Radial Basis Function Kernel and Hyperparameter Detection

Tomomasa Yamasaki, *Student Member, IEEE* , Zhehui Wang , Tao Luo, *Member, IEEE* ,  
Niangjun Chen, and Bo Wang, *Senior Member, IEEE* 

**Abstract**—Neural Architecture Search (NAS) is an automated technique to design optimal neural network architectures for a specific workload. Conventionally, evaluating candidate networks in NAS involves extensive training, which requires significant time and computational resources. To address this, training-free NAS has been proposed to expedite network evaluation with minimal search time. However, state-of-the-art training-free NAS algorithms struggle to precisely distinguish well-performing networks from poorly-performing networks, resulting in inaccurate performance predictions and consequently sub-optimal top-1 network accuracy. Moreover, they are less effective in activation function exploration. To tackle the challenges, this paper proposes RBFleX-NAS, a novel training-free NAS framework that accounts for both activation outputs and input features of the last layer with a Radial Basis Function (RBF) kernel. We also present a detection algorithm to identify optimal hyperparameters using the obtained activation outputs and input feature maps. We verify the efficacy of RBFleX-NAS over a variety of NAS benchmarks. RBFleX-NAS significantly outperforms state-of-the-art training-free NAS methods in terms of top-1 accuracy, achieving this with short search time in NAS-Bench-201 and NAS-Bench-SSS. In addition, it demonstrates higher Kendall correlation compared to layer-based training-free NAS algorithms. Furthermore, we propose NAFBee, a new activation design space that extends the activation type to encompass various commonly used functions. In this extended design space, RBFleX-NAS demonstrates its superiority by accurately identifying the best-performing network during activation function search, providing a significant advantage over other NAS algorithms.

**Index Terms**—Training-free, neural architecture search, Radial Basis Function, activation

## I. INTRODUCTION

OVER the past decade, Deep Neural Networks (DNNs) are intensively utilized in numerous Artificial Intelligence (AI) applications across a multitude of domains in computer vision [1], natural language processing [2], social network analysis [3], recommendation systems [4], etc. However, deploying DNNs to achieve high accuracy for a specific task can incur substantial time and effort when manually designing the network and identifying the optimal architectures and hyperparameters. Neural Architecture Search (NAS) has been proposed to address this challenge. Conventional NAS automates the process of architecture search by generating candidate networks and validating their accuracy with training [5]–[12]. However, this approach is computationally expensive as network training can take a vast amount of time, particularly when network architectures become deep and complex. For instance, a NAS algorithm leveraging reinforcement learning can

take 28 days with 800 GPUs to identify a well-performed DNN topology [5]. To speed up NAS and reduce computational cost, researchers have proposed various techniques. LightNAS [13] estimates candidate network potential based on the total training losses for several epochs, which can reduce the training cost. Another efficient approach is leveraging neural predictors with simple regression models rather than training actual networks. The models can adopt random forest [14], auto-encoder [15], or decision tree [16] method to forecast the network performance. However, the regression models in the neural predictors still require training to ensure good performance.

To mitigate the issue, gradient-based zero-cost proxies for NAS have been proposed to evaluate networks in their initial state without the need for full training. This method evaluates networks by analyzing the knowledge obtained from forward or backward propagation. One basic proxy is `grad_norm` [17], which aggregates the Euclidean norm of the gradients from a single minibatch of training data. `Snip` proxy [18] evaluates networks using a saliency metric computed at initialization based on a single minibatch of data, approximating the change in loss (e.g., cross-entropy loss) when a specific parameter is removed. Unlike `snip`, `synflow` proxy [19] simply calculates its loss as the product of all network parameters without using minibatch data and cross-entropy loss. `ZiCo` [20] estimates training convergence speed and generalization capacity based on the mean value and standard deviation of the gradients. `EProxy` [21] leverages a few-shot self-supervised regression to evaluate networks. Nonetheless, these gradient-based proxies are only effective for a restricted set of design spaces. In contrast, layer-based approaches do not require labels or loss values to predict the trained accuracy of a network, thus completely eliminating the training cost. For example, `TE-NAS` [22] analyzes the spectrum of the neural tangent kernel and the number of linear regions in the input space to score a network. `NASWOT` [23] provides a scoring system based on the difference in ReLU output among minibatches to predict the final trained accuracy, while `DAS` [24] further decouples the `NASWOT` scoring framework into distinguishing atomic and activation atomic metrics.

We propose RBFleX-NAS, a novel training-free NAS algorithm that further improves the scoring performance and extends the network design space to various activation functions. Our algorithm scores an individual network by examining the similarity of the activation outputs and the similarity of the

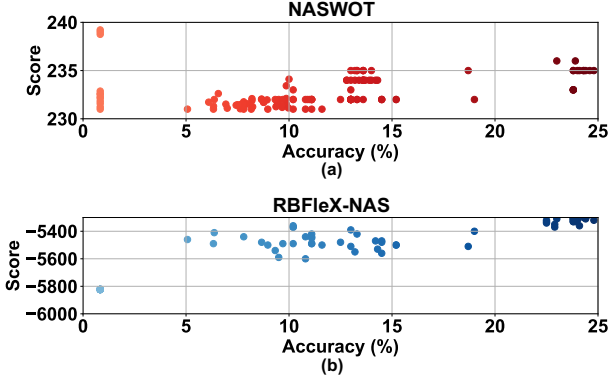


Fig. 1. The score vs. accuracy from (a) NASWOT and (b) proposed RBFleX-NAS when testing with NAS-Bench-201 over ImageNet. NASWOT cannot distinguish the network performance on the basis of their scores when the ground-truth accuracy on the ImageNet dataset falls below 25%. Note that the lighter the color, the lower the accuracy.

input feature maps of the last layer across different input images. This is because the last layer can play a key role in projecting the extracted features into lower dimensions by acting as a classifier [25]. Specifically, we exploit the Radial Basis Function (RBF) kernel to derive the similarity among images in a minibatch and predict the final trained accuracy of the network. Simultaneously, we develop a Hyperparameter Detection Algorithm (HDA), which searches for appropriate hyperparameters to assist the RBF kernels. We have validated that RBFleX-NAS achieves significantly higher Kendall correlation between scores and final trained accuracies of networks across widely used NAS benchmarks, including NAS-Bench-201 [26], NATS-Bench-SSS [27], NDS [28] as well as TransNAS-Bench-101 [29]. Our source code is available at <https://github.com/Edge-AI-Acceleration-Lab/RBFleX-NAS.git>. Our contributions are summarized as follows.

- We propose RBFleX-NAS, a zero-cost NAS algorithm that leverages the similarity of activation outputs and the similarity of the input feature maps of the last layer among input images. RBFleX-NAS is more precise in distinguishing network performance with scores, achieving higher top-1 accuracy in search.
- We propose NAFBee, a new design space for benchmarking purposes with VGG-19 and BERT, further extending the activation type from ReLU to various commonly used functions. RBFleX-NAS successfully identifies the best-performing network with activation function search, which the current NAS algorithms fail to do.
- We achieve significantly superior accuracy correlation in network scoring compared to state-of-the-art layer-based training-free NAS across various NAS benchmarks.

## II. PRIOR ARTS

A variety of techniques have been developed for network architecture search, such as reinforcement learning [5], [7], evolutionary algorithm [30], gradient algorithm [31], Deep Q

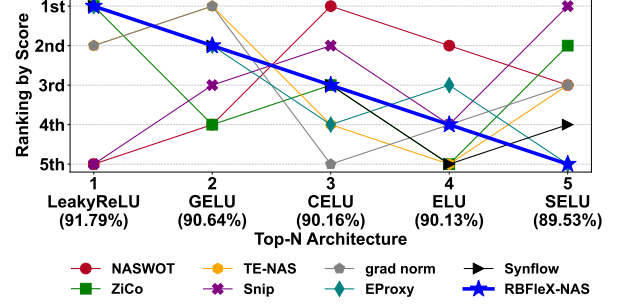


Fig. 2. Illustration of activation function exploration on VGG-11 with CIFAR-10 dataset. The Y-axis represents the accuracy ranking based on the score, which is evaluated by various training-free NAS methods using networks designed with five distinct non-ReLU activation functions.

Network (DQN) [32], etc. However, they all have to train the candidate networks for performance evaluation, rendering a large amount of computation time and GPU power.

Recently, layer-based NAS algorithms without training have been proposed to address the problem. The algorithms are completely training-free and thus do not need labels or loss information. For instance, NASWOT [23] and DAS [24] score candidate networks and correlate the scores to their final trained accuracy rather than train them directly. NASWOT evaluates the networks based on the difference in ReLU output among the images in a minibatch. Specifically, ReLU partitions the input feature maps into either an activated region when the input is positive or an inactivated region otherwise. NASWOT treats these regions as binary features and scores a network accordingly. When a network exhibits a substantial difference in ReLU output among the input images, NASWOT recognizes it as a well-performed architecture as it indicates that the network can respond well to the features of different images. DAS further decouples the score equation in NASWOT into a distinguishing atomic and an activation atomic. The distinguishing atomic capture the network’s capability to differentiate among different inputs, while the activation atomic takes the number of activation functions to simplify the comparison among networks. Compared to NASWOT, DAS runs faster with higher reliability for certain network design spaces.

However, NASWOT and DAS impose two limitations in scoring and design space. In the scoring phase, NASWOT and DAS merely check the ReLU output and the number of ReLU layers. However, the ReLU-related information is insufficient to predict the final accuracy of a network [25]. For instance, NASWOT can not distinguish the network performance based on their scores when the ground-truth accuracy of the ImageNet dataset falls below 25% (Fig. 1(a)). In particular, the two networks with an accuracy of 0.8% obtain even higher scores compared to the remaining candidates, manifesting inaccurate performance predictions by NASWOT. This is because the last layer (e.g., a Fully Connected layer with softmax) also plays a key role in projecting the extracted features into lower dimensions by acting as a classifier [25]. Moreover, Fig. 2 reveals that NASWOT exhibits a poor correlation between score and network accuracy across different activation

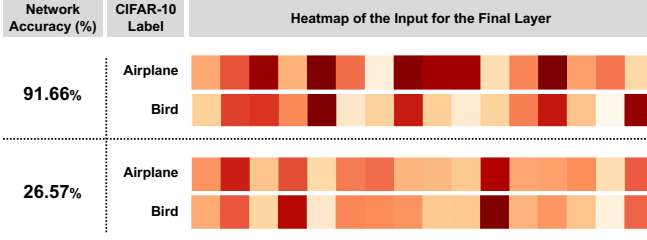


Fig. 3. Input heatmap of the last layer from a network with higher accuracy (91%) and a network with lower accuracy (26%) over CIFAR-10.

functions. Similarly, other state-of-the-art training-free NAS algorithms, including TE-NAS, grad\_norm, Synflow, Snip, ZiCo, and EProxy perform poorly in differentiating network accuracy attributed to different activation functions.

Hereby, we propose RBFlex-NAS, a novel algorithm that leverages RBF kernels with hyperparameter detection to forecast the final trained accuracy of the candidate networks by taking the last layer into account. Moreover, it enables activation function exploration in the design space, offering more flexibility for DNN design.

### III. METHOD

This section presents a detailed description of RBFlex-NAS for the network search. We begin by discussing our kernel-based approach and explaining how to measure the similarity. Next, we introduce HDA to obtain the fine-tuned hyperparameters for the RBF kernel. Subsequently, we elaborate on network initialization and the effect of minibatch size on determining a score. Finally, we discuss the impact of images in different batches.

#### A. Analyzing Networks using RBF Kernel

A critical factor contributing to the performance of RBFlex-NAS is its ability to analyze the full information of the feature maps in the network layers by RBF kernels with proposed HDA, as opposed to relying on the binary representations utilized by state-of-the-art layer-based methods such as NASWOT and TE-NAS. RBFlex-NAS enables a more detailed evaluation of the activation function outputs while simultaneously considering the inputs to the final layer, which are critical for determining the network's performance. The heatmap in Fig. 3 illustrates that networks with higher accuracy can generate more distinct input representations for the final layer compared to networks with lower accuracy. RBFlex-NAS effectively captures the critical distinctions, enabling it to more accurately evaluate and rank network performance.

NASWOT [23] reveals that a well-performed network architecture tends to have a lower similarity in terms of ReLU outputs among different input images. However, it is worth noting that a network can still exhibit low accuracy though its ReLU output shows low similarity. This is because the network performance is indicated not only by the activation layers but also by the last layer [25].

In this section, we score a network architecture by accounting for both the similarity among the activation outputs

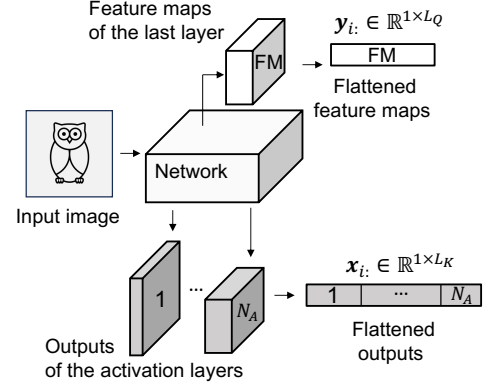


Fig. 4. Vector processing on RBFlex-NAS, where  $N_A$  is the number of activation functions.

and the similarity among the inputs of the last layer. Fig. 4 depicts the process of obtaining the output vector of the activation layer,  $\mathbf{x}_i \in \mathbb{R}^{1 \times L_K}$  and the input feature map vector of the last layer,  $\mathbf{y}_i \in \mathbb{R}^{1 \times L_Q}$ , where  $L_K$  and  $L_Q$  denote the length of these vectors, respectively. We flatten the activation output and input feature map vector for each input image. Specifically, we convert each three-dimensional output (i.e., width  $\times$  height  $\times$  channels) from an activation function into a one-dimensional vector and concatenate them horizontally to obtain the output vector. Similarly, we generate the input feature map vector by transforming the input feature maps into one dimension.

Fig. 5 shows the scoring process in our proposed RBFlex-NAS. Firstly, the framework generates  $N$  output vectors and  $N$  input feature map vectors based on the  $N$  input images in a minibatch. RBFlex-NAS then concatenates them vertically as an output matrix,  $\mathbf{X} \in \mathbb{R}^{N \times L_K}$  and an input feature map matrix,  $\mathbf{Y} \in \mathbb{R}^{N \times L_Q}$ , respectively. To better measure the similarity among different images, we normalize the two matrices with a range of  $0 \sim 1$ . There are three common matrix normalization techniques, namely element-wise normalization, row-wise normalization, and column-wise normalization, respectively. However, we observe the element-wise normalization and the row-wise normalization reduce the data correlation among rows in  $\mathbf{X}$  or  $\mathbf{Y}$ . Therefore, we adopt the column-wise normalization and illustrate the method with Equation (1).

$$\tilde{\alpha}_{ij} = \begin{cases} \frac{\alpha_{ij} - \min(\alpha_{:j})}{\max(\alpha_{:j}) - \min(\alpha_{:j})} & \text{if } \max(\alpha_{:j}) \neq \min(\alpha_{:j}) \\ \alpha_{ij} & \text{otherwise} \end{cases} \quad (1)$$

where  $\tilde{\alpha}_{ij}$  is the value after normalization,  $\alpha_{ij}$  is an element in  $\mathbf{X}$  or  $\mathbf{Y}$  and  $\alpha_{:j}$  denotes the  $j$ -th column vector of  $\mathbf{X}$  or  $\mathbf{Y}$ .

After obtaining the normalized matrices  $\tilde{\mathbf{X}}$  and  $\tilde{\mathbf{Y}}$ , we calculate the similarity matrices of the activation output  $\mathbf{K} \in \mathbb{R}^{N \times N}$  and the input feature maps  $\mathbf{Q} \in \mathbb{R}^{N \times N}$  by leveraging RBF kernel.

The RBF kernel is a non-linear function whose elements are representations of distance from the center, which is widely utilized in Support Vector Machine [33] [34], RBF networks [35], multi-task Gaussian process [36], etc as it can perform

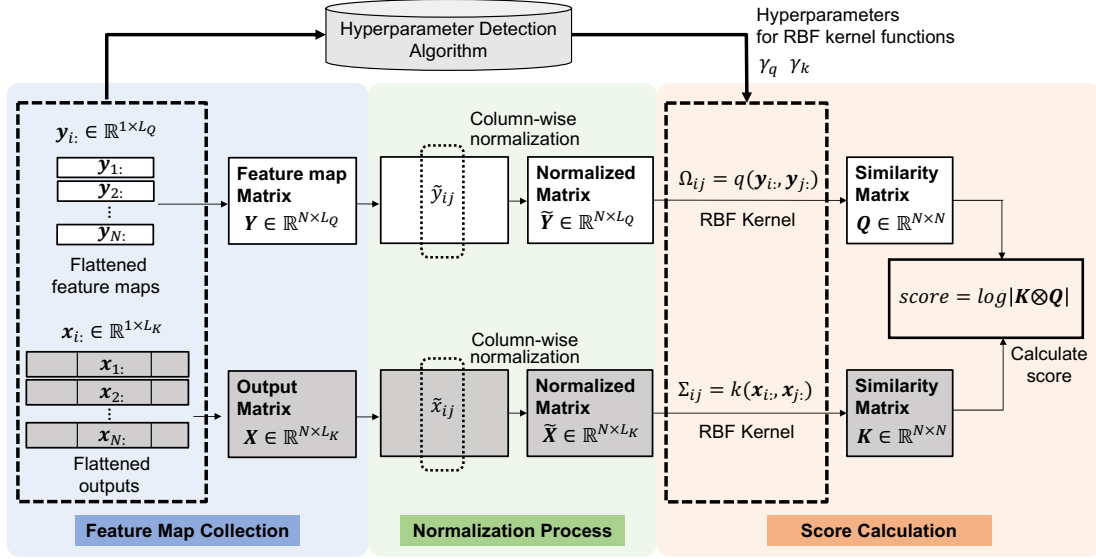


Fig. 5. The score computation process in RBFleX-NAS.

better in extracting complex features than many other kernels [37]. However, the RBF kernel is highly sensitive to the choice of hyperparameters. To address this issue, we develop an HDA which will be elaborated in Section III-B. Thanks to the HDA, we can obtain fine-tuned hyperparameters (i.e.,  $\gamma_k$  and  $\gamma_q$ ) to generate a precise similarity matrix. Specifically, each term in the similarity matrices (i.e.,  $\Sigma_{ij}$  and  $\Omega_{ij}$ ) is calculated with the RBF kernel as Equations (2) and (3) describe.

$$\Sigma_{ij} = \exp(-\gamma_k \|\tilde{\mathbf{x}}_i - \tilde{\mathbf{x}}_j\|^2) \quad (2)$$

$$\Omega_{ij} = \exp(-\gamma_q \|\tilde{\mathbf{y}}_i - \tilde{\mathbf{y}}_j\|^2) \quad (3)$$

Therefore, the similarity matrix of the activation outputs, denoted by  $\mathbf{K} \in \mathbb{R}^{N \times N}$ , and the similarity matrix of the last input feature maps, denoted by  $\mathbf{Q} \in \mathbb{R}^{N \times N}$ , can be represented as follows.

$$\mathbf{K} = \begin{pmatrix} \Sigma_{11} & \cdots & \Sigma_{1N} \\ \vdots & \ddots & \vdots \\ \Sigma_{N1} & \cdots & \Sigma_{NN} \end{pmatrix} \quad (4)$$

$$\mathbf{Q} = \begin{pmatrix} \Omega_{11} & \cdots & \Omega_{1N} \\ \vdots & \ddots & \vdots \\ \Omega_{N1} & \cdots & \Omega_{NN} \end{pmatrix} \quad (5)$$

A small value of  $\Sigma_{ij}$  or  $\Omega_{ij}$  reveals that the similarity is low between the  $i$ -th vector and the  $j$ -th vector in  $\tilde{\mathbf{X}}$  and  $\tilde{\mathbf{Y}}$ , respectively. Furthermore, a potentially good network tends to possess low similarity in both  $\mathbf{K}$  and  $\mathbf{Q}$  among various input images. As the matrices  $\mathbf{K}$  and  $\mathbf{Q}$  denote different similarities from the perspective of distinct layers, we exploit the Kronecker product  $\otimes$  to integrate the two matrices into one Figure-of-Merit for our scoring process. Specifically, we score a given network with the Kronecker product as Equation (6) shows. A higher score indicates a network with a higher accuracy.

$$score = \log |\mathbf{K} \otimes \mathbf{Q}| \quad (6)$$

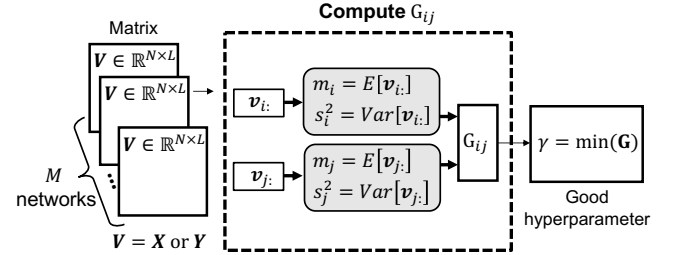


Fig. 6. Illustration of the proposed hyperparameter detecting algorithm in RBFleX-NAS.

Here we can further simplify Equation (6) to

$$score = N * (\log |\mathbf{K}| + \log |\mathbf{Q}|) \quad (7)$$

Consequently, the computational complexity of the score calculation becomes  $O(N^{2.373})$  according to the method in [38].

### B. Hyperparameter Detecting Algorithm (HDA)

The efficacy of the RBF kernel is largely subject to the value of hyperparameters such as  $\gamma_k$ ,  $\gamma_q$  in Equations (2) and (3). Therefore, fine-tuning hyperparameters is crucial for the performance of the proposed algorithm. A large number of applications employ costly methods such as grid search [39] to find the optimal hyperparameters. To minimize the cost, [40] leverages the method proposed in [41] to set appropriate hyperparameters when deploying the RBF kernel in Support Vector Machine. The approach derives a projection vector on the basis of Fisher Linear Discriminant (FLD), which can generate an optimal regression line to separate the observed data samples into two non-overlapped classes. As our work aims to evaluate the similarity among  $N$  input images, we develop an HDA inspired by FLD. Fig. 6 illustrates the algorithm. First, we select  $M$  candidate networks and obtain the output matrix  $\mathbf{X}$  and the input feature map matrix  $\mathbf{Y}$  for



each network using  $N$  input images. Next, for any two vectors  $\mathbf{v}_i$  and  $\mathbf{v}_j$  in  $\mathbf{X}$  or  $\mathbf{Y}$ , we define the mean value of the two vectors as

$$m_i = \frac{1}{L} \sum_{z=1}^L v_{iz} \quad (8)$$

$$m_j = \frac{1}{L} \sum_{z=1}^L v_{jz} \quad (9)$$

where  $L$  denotes the length of the vectors,  $v_{iz}$  and  $v_{jz}$  represent the  $z$ -th value in the selected vectors  $\mathbf{v}_i$  and  $\mathbf{v}_j$ , respectively. We then define the squared error of the mean value of two vectors  $D_{ij}$  as

$$D_{ij} = (m_i - m_j)^2 \quad (10)$$

However, evaluating the squared error between vectors solely by their mean values is not able to accurately assess their degree of overlap. As Fig.7 shows, the similarity between the vectors  $\mathbf{v}_i$  and  $\mathbf{v}_j$  from two entirely distinct input images is usually small and associated with much smaller variances (i.e.,  $s_i$  and  $s_j$ ) than the squared error  $D_{ij}$ . If one of the variances (e.g.,  $s'_i$ ) is close to or larger than  $D_{ij}$ , the similarity will increase. Therefore, we take the variance of the data samples in the two vectors into account. The variances of the two vectors are defined as

$$s_i^2 = \frac{1}{L} \sum_{z=1}^L (v_{iz} - m_i)^2 \quad (11)$$

$$s_j^2 = \frac{1}{L} \sum_{z=1}^L (v_{jz} - m_j)^2 \quad (12)$$

We define  $G_{ij}$  as a candidate hyperparameter for the RBF kernel, which is described as

$$G_{ij} = \frac{D_{ij}}{2(s_i^2 + s_j^2)} \quad \text{if } D_{ij} \neq 0 \quad (13)$$

Specifically, the candidate hyperparameter matrices  $\mathbf{G}_k$  and  $\mathbf{G}_q$  are defined by Equation (13), where the former is the hyperparameter matrix for the similarity of activation outputs and the latter is the matrix for the input feature maps of the last layer.

Fig.8 illustrates the RBF kernel function with different hyperparameter values, where the grey zone indicates the range of Euclidean distance  $\|\mathbf{v}_i - \mathbf{v}_j\|$ . A very large hyperparameter can make RBF kernel in Equation (2) and (3) insensitive to the difference in  $\|\mathbf{v}_i - \mathbf{v}_j\|$ , where  $\mathbf{v}$  is  $\mathbf{x}$  or  $\mathbf{y}$ . Thus the hyperparameters,  $\gamma_k$  and  $\gamma_q$ , should not be either too large or too small and an optimal hyperparameter is favorable to distinguish the similarity from various input images (i.e., with sufficient score variance). In particular, the following equation

$$\gamma = \frac{\log(1/\epsilon)}{\max_{i,j} \|\mathbf{v}_i - \mathbf{v}_j\|^2} \quad (14)$$

guarantees that  $\exp(-\gamma \|\mathbf{v}_i - \mathbf{v}_j\|^2) = \epsilon$  when  $\|\mathbf{v}_i - \mathbf{v}_j\|^2$  becomes the largest and  $\exp(-\gamma \|\mathbf{v}_i - \mathbf{v}_j\|^2) = \epsilon^{1/r}$  when  $\|\mathbf{v}_i - \mathbf{v}_j\|^2$  becomes the smallest, where  $r = \frac{\max_{i,j} \|\mathbf{v}_i - \mathbf{v}_j\|^2}{\min_{i,j} \|\mathbf{v}_i - \mathbf{v}_j\|^2}$  and we can choose an  $\epsilon$  such that  $[\epsilon, \epsilon^{1/r}]$  is as wide as

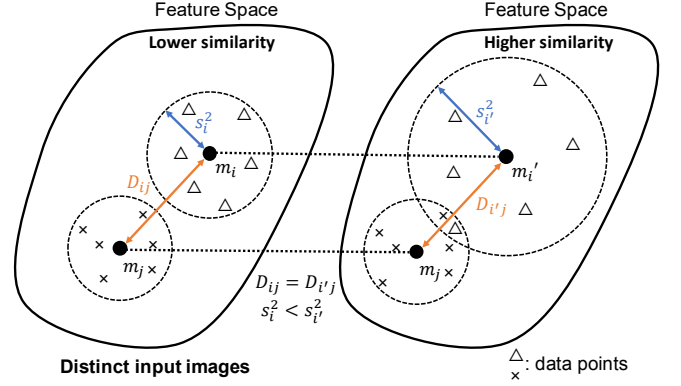


Fig. 7. Illustration of distinct input images that exhibit low similarity with small variance.  $D_{ij}$  and  $D'_{ij}$  are the squared error of the mean value between  $m_i$  and  $m_j$  as well as between  $m'_i$  and  $m'_j$ , respectively.  $s_i$  and  $s'_i$  are the variances of data points, respectively.

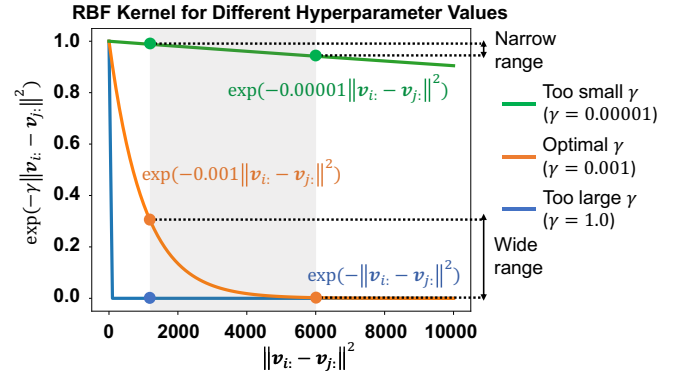


Fig. 8. RBF kernel for different hyperparameter values. The grey square indicates the range of Euclidean distance.

possible. Therefore, in RBFlex-NAS, the fine-tuned hyperparameter  $\gamma_k$  and  $\gamma_q$  are obtained by the entry-wise minimal value in respective  $\mathbf{G}_k$  and  $\mathbf{G}_q$  as follows, where  $\gamma_k > 0$ ,  $\gamma_q > 0$  and  $\min_{i,j} \mathbf{G}(i,j)$  denotes the minimum entry in the matrix  $\mathbf{G}$ .

$$\gamma_k = \min_{i,j} \mathbf{G}_k(i,j) \quad \text{where } D_{ij}^k \neq 0 \quad (15)$$

$$\gamma_q = \min_{i,j} \mathbf{G}_q(i,j) \quad \text{where } D_{ij}^q \neq 0 \quad (16)$$

#### IV. EXPERIMENTAL RESULT

We perform experiments to evaluate the efficacy of the proposed RBFlex-NAS in this section. Firstly, we investigate the effect of network initialization, minibatch size, and image batch on our score. Next, we compare the RBF kernel method with other similarity assessment methods. Thirdly, we evaluate the hyperparameter detecting algorithm. Subsequently, we compare RBFlex-NAS with gradient-based training-free NAS (i.e., grad\_norm [17], snip [18], synflow [19], ZiCo [20], and EProxy [21]) and layer-based training-free NAS (i.e., NASWOT [23], TE-NAS [22], and DAS [24]) in terms of the correlation between the score and the network accuracy. Afterwards, we discuss the top-1 searched network in design spaces. Finally, we verify that RBFlex-NAS can

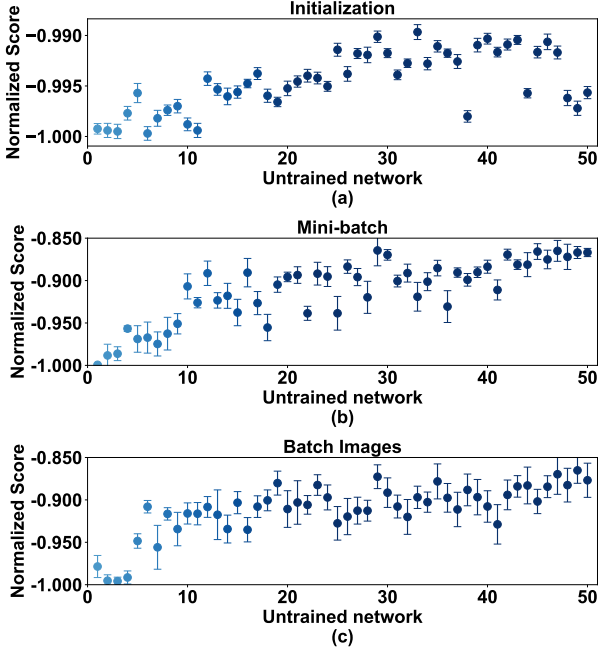


Fig. 9. Normalized network scores on NATS-Bench-SSS with respect to (a) network initialization, (b) minibatch size, and (c) different image batches. 50 networks are randomly sampled from NATS-Bench-SSS and ranked with its accuracy. The first untrained network exhibits the lowest accuracy, while the 50th network achieves the highest accuracy. The normalized score is obtained by dividing each network’s score by the minimum score derived from the first untrained network. As the RBFlex score is inherently negative, the normalized score starts at -1.0. A more negative normalized score corresponds to a better-performed network.

score networks with various types of activation functions, leading to extended design space with activation function exploration. All computations in RBFlex-NAS are performed using 64-bit floating point precision to avoid the diminishing of similarity information when the associated hyperparameter value becomes too small. We utilize NAS-Bench-201 [26], NATS-Bench [27], and Network Design Space (NDS) [28] for the experiments on image classification workloads, and TransNAS-Bench-101 [29] for object classification and semantic segmentation. Specifically, NAS-Bench-201 consists of 15,625 networks pre-trained on CIFAR-10, CIFAR-100, and ImageNet. NATS-Bench integrates NATS-Bench-SSS for network size benchmarking and NATS-Bench-TSS for network topology exploration. NDS provides a variety of NAS search spaces, such as ResNet, Amoeba, DARTS, ENAS, PNAS, and NASNet. TransNAS-Bench-101 provides 3,256 networks in macro-level search space with different depths, down-sampling layers, and enlarged-channel layers. It also incorporates 4,096 networks in micro-level (i.e., cell-level) search space with different operations adapting the feature map from node to node. These networks are pre-trained with the Taskonomy dataset [42]. For the experiment on activation function design space, we create the Neural Network Activation Function Benchmark (NAFBee) based on VGG-19 over CIFAR-10 dataset and BERT over SST-2 dataset. NAFBee is available at <https://github.com/Edge-AI-Acceleration-Lab/NAFBee.git>

#### A. Impact of Network Initialization on RBFlex-NAS

RBFlex-NAS initializes the weights of a network before scoring it. The network initialization can play a significant role in its final accuracy [43], [44]. To investigate the effect of the initialization on the network performance, we randomly select 50 networks from a variety of network design space benchmarks, which are NATS-Bench-SSS [27], NAS-Bench-201 [26], NDS(Amoeba) [28], NDS(DARTS), NDS(ENAS), and NDS(PNAS), respectively. We initialize their weights with random values and then score all selected networks 10 times with the ImageNet dataset. We investigate the effect of the network initialization via the score with min-max normalization on each trial.

Fig. 9(a) reveals the result from NATS-Bench-SSS. The accuracy of the untrained networks is exhibited in increasing order. Specifically, the first untrained network shows the lowest accuracy, while the 50th network achieves the highest accuracy. Apparently, RBFlex-NAS can consistently distinguish the networks in NATS-Bench-SSS with a negligible standard deviation of the score (i.e., standard deviation ranges from  $\pm 4.1 \times 10^{-4}$  to  $\pm 8.2 \times 10^{-4}$ ). We also validate the network initialization in other design spaces and have observed a small standard deviation of  $5.2 \times 10^{-3}$  for NAS-Bench-201,  $1.6 \times 10^{-2}$  for NDS(Amoeba),  $2.8 \times 10^{-3}$  for NDS(DARTS),  $1.3 \times 10^{-2}$  for NDS(ENAS), and  $3.4 \times 10^{-3}$  for NDS(PNAS), respectively. Therefore, our scoring approach is effective regardless of the initial weight values.

#### B. Impact of Minibatch Size on RBFlex-NAS

In the network scoring phase, RBFlex-NAS processes all the images in the same minibatch concurrently. We investigate the effect of the minibatch size by randomly selecting 50 networks from our design space benchmarks while ensuring distinct accuracy values. Subsequently, we score each network with a variety of batch sizes over the ImageNet dataset and normalize the scores to visualize the impact.

Fig. 9(b) shows the normalized score for minibatch size using NATS-bench-SSS. A larger normalized score indicates a better-performed network. RBFlex-NAS can successfully identify good architectures with a mean normalized score above -0.85 against different minibatch sizes. Tested with NAS-Bench-201 and NDS, RBFlex-NAS can evaluate the networks with very small standard deviations, which are less than  $2.7 \times 10^{-2}$  in NAS-Bench-201,  $8.1 \times 10^{-3}$  in NDS(Amoeba),  $4.4 \times 10^{-3}$  in NDS(DARTS),  $6.3 \times 10^{-3}$  in NDS(ENAS), and  $4.9 \times 10^{-3}$  in NDS(PNAS). The tiny standard deviation indicates that RBFlex-NAS can consistently differentiate networks with distinct levels of accuracy in a design space, regardless of the minibatch size  $N$ .

#### C. Impact of Image Batch on RBFlex-NAS

RBFlex-NAS randomly selects  $N$  images from a dataset to score a network. We thus analyze the effect of the image batch by selecting 50 networks from each benchmark (i.e., NATS-Bench-SSS, NAS-Bench-201, and NDS). RBFlex-NAS scores a network with 10 different batches on the ImageNet dataset.

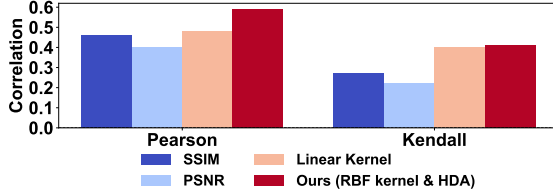


Fig. 10. Pearson and Kendall Correlation of various similarity assessment methods. HDA detects the hyperparameter for RBF kernel.

We group 16 random images as a minibatch and score each network with 10 minibatches. We then investigate the effect of image batch with the same score normalization technique on each trial.

Fig. 9(c) illustrates the result of NATS-Bench-SSS with various image batches. The standard deviation of the score ranges from  $\pm 4.6 \times 10^{-3}$  to  $\pm 2.9 \times 10^{-2}$ , which is significantly smaller than the score variance. Besides, RBFleX-NAS can also evaluate the networks from NAS-Bench-201 and NDS with small standard deviations, which are less than  $2.8 \times 10^{-2}$  for NAS-Bench-201,  $1.4 \times 10^{-3}$  for NDS(Amoeba),  $1.1 \times 10^{-3}$  for NDS(DARTS),  $1.9 \times 10^{-3}$  for NDS(ENAS), and  $1.8 \times 10^{-3}$  for NDS(PNAS), respectively. Therefore, RBFleX-NAS can effectively evaluate network architectures regardless of the image batch.

#### D. Comparative Analysis of Similarity Assessment Methods

RBFleX-NAS utilizes RBF kernels to assess the similarities among feature maps from a network. This experiment compares RBF kernel with other similarity assessment methods, such as linear kernel [45], the Peak Signal-to-Noise Ratio (PSNR) [46], and the Structural Similarity Index Measure (SSIM) [47]. We randomly sample 1000 untrained networks from NATS-Bench-SSS and score those networks based on the four methods. Pearson and Kendall correlation coefficients are widely adopted to indicate the strength of the relationship between two variables [48] [23]. We thus compare these similarity assessment methods by using mean Pearson and Kendall correlation coefficients over 10 sets of 1000 sampled networks. Our HDA derives the hyperparameters for RBF kernels. We score networks by CIFAR-10 dataset with a minibatch size of 16 and a number of networks for HDA of 10 (i.e.,  $N = 16$ ,  $M = 10$ ).

Fig. 10 reveals the RBF kernel method exhibits the highest mean Pearson correlation of 0.59 while the linear kernel method, PSNR, and SSIM yielded lower mean Pearson correlations of 0.48, 0.40 and 0.46, respectively. In terms of Kendall correlation, the RBF kernel method again achieves the highest mean Kendall correlation of 0.41. The linear kernel method, PSNR, and SSIM exhibit lower correlations of 0.40, 0.22, and 0.27, respectively. We confirm that the RBF kernel with HDA can effectively evaluate the similarity among feature maps.

#### E. Evaluation of HDA

To evaluate HDA, we randomly sample 1000 untrained networks from NATS-Bench-SSS and calculate the score of

each network with the fine-tuned hyperparameters obtained from the algorithm. We repeat this process 10 times over the CIFAR-10 dataset. To evaluate the performance of our HDA, we deploy Pearson correlation coefficient and Kendall correlation coefficient. Moreover, we compare our HDA with other two hyperparameter-detecting methods. Specifically, the first comparison method selects the maximal value in the candidate hyperparameter matrix  $\mathbf{G}_k$  and  $\mathbf{G}_q$ , respectively while the second method randomly set values between  $10^{-1}$  and  $10^{-20}$ . We consistently configure the minibatch size  $N$  as 16, and the number of candidate networks  $M$  as 10.

Fig. 11 depicts the results of our HDA through a box-and-whisker plot, with mean Pearson and Kendall correlation values of 0.56 and 0.39, respectively. If selecting the maximal values in  $\mathbf{G}_k$  and  $\mathbf{G}_q$  for the hyperparameters as the first method, the mean correlations decrease to 0.43 and 0.26, respectively. Alternatively, if randomly setting the hyperparameters as the second method, the corresponding correlation values drop to 0.46 and 0.27, respectively. We conduct a  $T$ -Test to assess the statistical difference between HDA and the maximum value as  $T$ -Test is a statistical test widely adopted to compare the mean of two groups [49] [50].  $P$ -value calculated on  $T$ -Test indicates the mean difference for two groups is statistically significant if  $P$ -value is lower than 0.05. The results show a  $P$ -value of  $2.1 \times 10^{-5}$  for the Pearson correlation and  $1.7 \times 10^{-10}$  for the Kendall correlation. Similarly, when comparing HDA with the random selection, the  $T$ -Test yields a  $P$ -value of  $5.0 \times 10^{-4}$  for the Pearson correlation and  $6.6 \times 10^{-7}$  for the Kendall correlation. As the  $P$ -value is smaller than 0.05, we confirm that the proposed HDA is statistically significant to select better hyperparameters  $\gamma_k$  and  $\gamma_q$  for the RBF kernel.

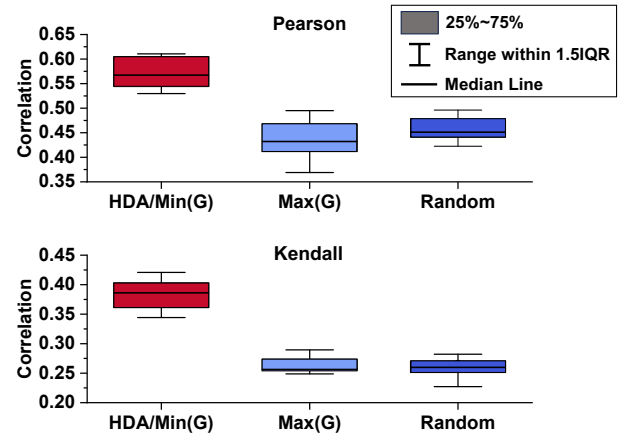


Fig. 11. Pearson and Kendall correlations with hyperparameter detection algorithm (HDA) and random hyperparameters. The minibatch size is 16.

#### F. Evaluation of correlations between score and accuracy

In this experiment for image classification tasks, we compare RBFleX-NAS with eight NAS algorithms. Specifically, we benchmark it with gradient-based algorithms, including grad\_norm [17], snip [18], synflow [19], EProxy [21], and ZiCo [20]. Simultaneously, we benchmark it with layer-

TABLE I  
PEARSON AND KENDALL CORRELATION ON NAS-BENCH-201 AND NATS-BENCH-SSS

Search Space	Method Metric	Name	Pearson Correlation			Kendall Correlation		
			CIFAR-10	CIFAR-100	ImageNet	CIFAR-10	CIFAR-100	ImageNet
NAS Bench 201	Gradient-based (requires loss or labels)	grad_norm	-0.009	0.034	0.087	0.170	0.204	0.220
		snip	0.003	0.049	0.033	0.174	0.212	0.366
		synflow	0.024	0.050	0.137	0.296	0.346	0.224
		EProxy	-0.280	-0.878	-0.618	-0.426	-0.528	-0.469
		ZiCo	0.529	0.636	0.734	0.564	0.603	0.583
	Layer-based (no loss and label required)	DAS	0.717	0.636	0.582	0.372	0.406	0.374
		NASWOT	0.727	0.638	0.575	0.374	0.407	0.376
		TE-NAS	0.051	0.095	0.266	0.168	0.127	0.033
		<b>RBFlEX-NAS</b>	<b>0.898</b>	<b>0.723</b>	<b>0.514</b>	<b>0.569</b>	<b>0.590</b>	<b>0.513</b>
NATS Bench SSS	Gradient-based (requires loss or labels)	grad_norm	0.606	0.437	0.494	0.426	0.317	0.376
		snip	0.698	0.531	0.669	0.511	0.394	0.523
		synflow	0.508	0.453	0.560	0.718	0.579	0.771
		EProxy	-0.346	0.376	0.166	-0.237	0.279	0.130
		ZiCo	0.907	0.738	0.871	0.729	0.555	0.697
	Layer-based (no loss and labels required)	DAS	0.484	0.241	0.523	0.318	0.159	0.366
		NASWOT	0.484	0.241	0.524	0.318	0.160	0.367
		TE-NAS	-0.146	-0.151	-0.363	-0.114	-0.122	-0.313
		<b>RBFlEX-NAS</b>	<b>0.607</b>	<b>0.855</b>	<b>0.869</b>	<b>0.419</b>	<b>0.639</b>	<b>0.649</b>

based methods, including NASWOT [23], DAS [24], and TE-NAS [22]. We test on various datasets, including CIFAR-10, CIFAR-100, and ImageNet, as well as with different network design spaces such as NAS-Bench-201, NATS-Bench-SSS, NDS(Amoeba), NDS(DARTS), NDS(ENAS), NDS(PNAS), NDS(ResNet), and NDS(NASNet). We configure the mini-batch size  $N$  as 16 and use 10 networks as the parameter  $M$  to detect appropriate hyperparameters for RBF kernels. We also deploy the same two correlation coefficients and  $T$ -test to verify the statistical significance.

To compare the performance of RBFlEX-NAS with the benchmarks, we conduct experiments on NAS-Bench-201, NATS-Bench-SSS, and NDS(ResNet), each with more than 10,000 networks. We randomly sample 1000 untrained networks and calculate the score of each network using RBFlEX-NAS and the benchmarks. We repeat this process 10 times and compute the mean correlations for each algorithm. For design spaces with fewer networks (i.e., NDS(Amoeba), NDS(DARTS), NDS(ENAS), NDS(PNAS) and NDS(NASNet)), we deploy the NAS algorithms to evaluate in each design space.

We further evaluate RBFlEX-NAS on object classification and semantic segmentation tasks using TranNAS-Bench-101 [29] and Taskonomy dataset [42]. Specifically, we compare RBFlEX-NAS with seven state-of-the-art training-free NAS algorithms, which are EProxy, TE-NAS, ZiCo, NASWOT, grad\_norm, snip, and synflow. RBFlEX-NAS employs a mini-batch size  $N$  of 16 and utilizes 10 networks for HDA. All algorithms in the experiment score 3,256 networks in the macro-level design space and 4,096 networks in the micro-level design space. Pearson and Kendall correlations are calculated to evaluate the relationship between the scores and actual accuracies.

Table I shows the experiment results on NAS-Bench-201 and NATS-Bench-SSS over CIFAR-10, CIFAR-100, and ImageNet. Fig. 12 shows the Pearson and Kendall correlation on NDS benchmark over CIFAR-10 and ImageNet. Though RBFlEX-NAS exhibits lower correlation than ZiCo in certain

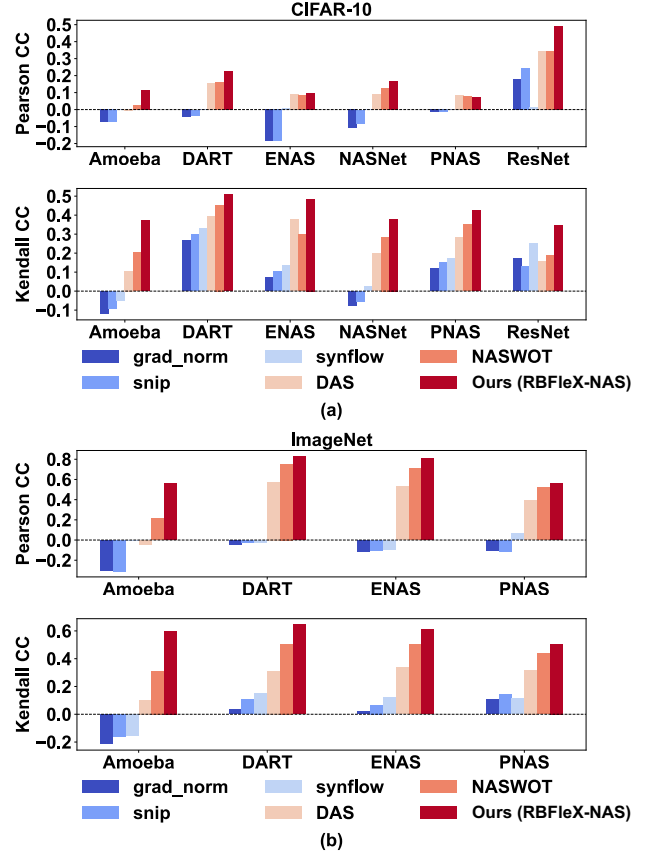


Fig. 12. Pearson and Kendall Correlations on NDS benchmark. (a) over CIFAR-10. (b) over ImageNet

cases, it can identify networks with higher accuracy using less search time, which will be elaborated in Section IV-G. Moreover, it shows higher Kendall correlations compared to all layer-based training-free NAS methods, including DAS, NASWOT and TE-NAS across both search spaces. For NATS-Bench-SSS, our RBFlEX-NAS also outperforms layer-based training-free algorithms (i.e., NASWOT, DAS, and TE-NAS)



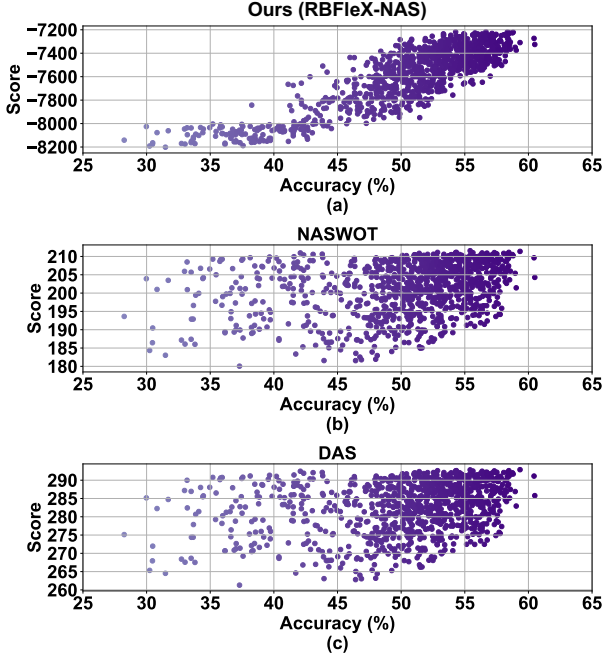


Fig. 13. Score vs final accuracy over CIFAR-100 in NATS-Bench-SSS with a minibatch size of 16. (a) Score by RBFlex-NAS. (b) Score by NASWOT. (c) Score by DAS.

in terms of Pearson correlation. Fig. 12(a) illustrates that RBFlex-NAS consistently outperforms state-of-the-art layer-based and gradient-based training-free NAS methods in NDS over CIFAR-10, as it achieves higher positive correlations across all design spaces. In contrast, the gradient-based proxies which are evaluated on NDS(Amoeba) and NDS(NASNet) show negative Kendall correlations.

In terms of the Pearson and Kendall correlation over CIFAR-100, our RBFlex-NAS outperforms other layer-based and gradient-based algorithms significantly in NATS-Bench-SSS, achieving a higher Pearson correlation of 0.855 and a higher Kendall correlation of 0.639. The experiment on NATS-Bench-SSS over ImageNet shows that RBFlex-NAS demonstrates apparently higher correlations compared to other layer-based training-free NAS frameworks. Specifically, the Pearson and Kendall correlations are 0.869 and 0.649, respectively, despite the increased challenge posed by the ImageNet dataset.

Fig. 12(b) shows RBFlex-NAS also achieves higher correlation for all design space from NDS while grad\_norm, snip, and synflow proxies achieve negative Kendall correlation for NDS(Amoeba). From the data in the tables, we observe that RBFlex-NAS can achieve a positive correlation between the score and the final accuracy of the networks. Moreover, we highlight the better results from RBFlex-NAS, which reveals that RBFlex-NAS outperforms NASWOT and DAS in predicting the final trained accuracy of the networks. Besides, RBFlex-NAS demonstrates positive correlations across all design spaces, while the gradient-based proxies yield negative correlations for NDS design spaces, indicating RBFlex-NAS’s versatility.

Fig. 13 shows the scatter plots between the score and the validated accuracy of the networks over CIFAR-100 in

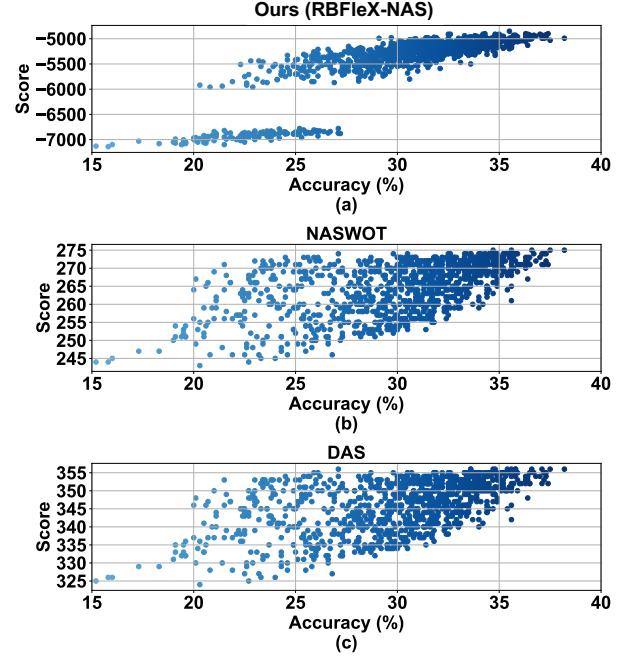


Fig. 14. Score vs final accuracy over ImageNet in NATS-Bench-SSS with a minibatch size of 16. (a) Score by RBFlex-NAS. (b) Score by NASWOT. (c) Score by DAS.

NATS-Bench-SSS by RBFlex-NAS, NASWOT, and DAS, respectively. RBFlex-NAS successfully evaluates the underperforming networks with an accuracy below 40% and effectively distinguishes them from other well-performed candidates. RBFlex-NAS also demonstrates a more linear dependency between the score and the accuracy of the networks compared to NASWOT and DAS.

Fig. 14 exhibits the dependency between the score and the final accuracy of the networks from NATS-Bench-SSS over the ImageNet dataset. The plot shows that RBFlex-NAS outperforms NASWOT and DAS in identifying better-performed networks. Specifically, RBFlex-NAS is able to distinguish better networks (i.e., accuracy higher than 30%) from inferior networks (i.e., accuracy between 15%-25%) while NASWOT and DAS can assign almost the same score to the networks with a lower accuracy (i.e., between 20% and 30%) and the networks with significantly higher accuracy (i.e., 30% or above).

Table II shows Pearson and Kendall correlations on object classification and semantic segmentation tasks using TransNAS-Bench-101. On macro-level object classification (OC Macro), RBFlex-NAS achieves a higher accuracy of 45.42% with higher Pearson and Kendall correlations. On micro-level object classification (OC Micro), RBFlex-NAS also exhibits a higher accuracy of 43.26% with a higher Kendall correlation compared to TE-NAS and NASWOT. For macro-level semantic segmentation (SS Macro), the Pearson and Kendall correlations of RBFlex-NAS are 0.853 and 0.668 with the highest mIoU of 29.15%. For micro-level semantic segmentation (SS Micro), RBFlex-NAS achieves a Pearson correlation of 0.547 and a Kendall correlation of 0.381 with the highest mIoU of 25.33%. This illustrates that RBFlex-NAS

TABLE II  
PEARSON AND KENDALL CORRELATION FOR OBJECT CLASSIFICATION  
(OC) AND SEMANTIC SEGMENTATION (SS) TASKS USING  
TRANSNAS-BENCH-101.

Search Space	Method Metric	Name	Correlation Pearson	Kendall	Top-1 (%)
OC Macro	Gradient-based	grad_norm	-0.291	-0.194	44.43
		snip	0.073	0.009	44.49
		synflow	-0.788	-0.586	42.42
		EProxy	-0.026	-0.049	44.28
		ZiCo	-0.167	-0.110	43.45
	Layer-based	TE-NAS	0.011	-0.029	45.02
		NASWOT	0.734	0.554	45.42
		<b>RBFLex-NAS</b>	<b>0.740</b>	<b>0.555</b>	<b>45.42</b>
		grad_norm	0.130	0.094	38.40
		snip	0.068	0.407	42.26
OC Micro	Gradient-based	synflow	0.035	0.102	26.55
		EProxy	-0.008	-0.019	40.15
		ZiCo	0.632	0.398	43.05
	Layer-based	TE-NAS	-0.030	-0.045	42.57
		NASWOT	0.598	0.322	27.93
		<b>RBFLex-NAS</b>	<b>0.461</b>	<b>0.338</b>	<b>43.26</b>
SS Macro	Gradient-based	grad_norm	-0.125	-0.083	28.07
		snip	0.059	0.029	28.57
		synflow	-0.765	-0.57	21.05
		EProxy	-0.049	-0.062	21.18
		ZiCo	-0.087	-0.063	26.79
	Layer-based	TE-NAS	-0.002	0.001	24.85
		NASWOT	0.854	0.674	29.15
		<b>RBFLex-NAS</b>	<b>0.853</b>	<b>0.668</b>	<b>29.15</b>
SS Micro	Gradient-based	grad_norm	0.216	0.385	22.68
		snip	0.098	0.488	24.43
		synflow	0.035	0.230	5.41
		EProxy	-0.036	-0.037	15.25
		ZiCo	0.620	0.416	24.43
	Layer-based	TE-NAS	-0.015	-0.115	9.34
		NASWOT	0.592	0.339	21.87
		<b>RBFLex-NAS</b>	<b>0.547</b>	<b>0.381</b>	<b>25.33</b>

is capable of identifying higher-accuracy networks with good correlation in object classification and semantic segmentation.

### G. Analysis of Architecture Search

This experiment compares the accuracies and search costs of the best networks (i.e., the networks with the highest score) identified by RBFLex-NAS and other state-of-the-art gradient-based and layer-based training-free NAS methods in NAS-Bench-201, NATS-Bench-SSS, and DARTS design space. To evaluate them on NAS-Bench-201 and NATS-Bench-SSS, we randomly sample a total of  $S$  networks from each design space. We perform architecture search following the methodology in NASWOT. Specifically, we firstly work with the CIFAR-10 dataset for NAS-Bench-201 and select the network with the highest score. In the next scoring phase, we evaluate the accuracy of the selected network over CIFAR-10, CIFAR-100, and ImageNet, resulting in identical search time across datasets. For NATS-Bench-SSS, networks are selected and scored separately for CIFAR-10, CIFAR-100, and ImageNet. The accuracy of each network is then evaluated on the respective dataset, resulting in different search time across datasets. For  $S = 10$  and  $S = 100$ , the accuracy metrics for ZiCo, Synflow, Grad Norm, and NASWOT are averaged over 500 runs to ensure statistical robustness. However, TE-NAS

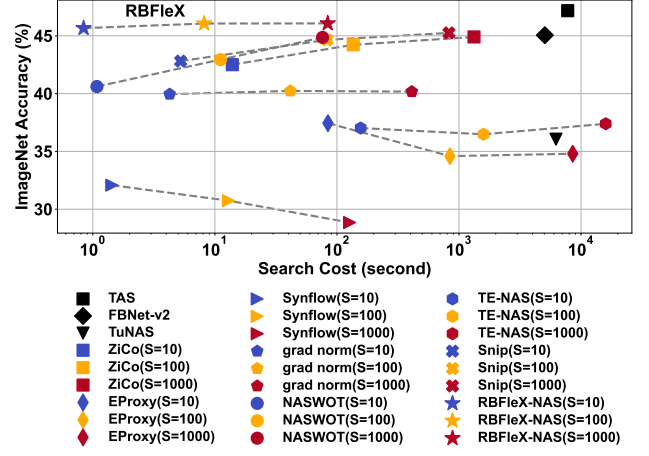


Fig. 15. Search cost versus network accuracy in ImageNet classification on NATS-Bench-SSS.

and EProxy are averaged over 50 runs due to computational limitations. For  $S = 1000$ , the accuracy metrics for all gradient-based and layer-based training-free NAS methods are averaged over 50 runs, except for TE-NAS and EProxy, which are averaged over 5 runs, also due to computational limitations.

Besides, we evaluate other common NAS algorithms such as Random Search with Parameter Sharing (RSPS) [51], DART [31], GDAS [52], ENAS [7], SETN [53], TAS [54], FBNet-v2 [55], and TuNAS [56] and compare them with RBFLex-NAS. Specifically, we randomly select 500 networks from their respective design space and calculate the average accuracy. In the DARTS design space, RBFLex-NAS evaluates all 5,000 networks. We train the top-1 scored network for 800 epochs with a batch size of 96 to align with the evaluation method used by the benchmark algorithms. The remaining parameters are configured the same as those in the DARTS papers [31]. Besides, we also evaluate ZiCo [20], TE-NAS [22], P-DARTS [57], PC-DARTS [58], ENAS [7], GDAS [52], DARTS-v1 [31], and PNAS [59]. We employ a single NVIDIA Tesla V100 GPU for all computations to implement this experiment.

Table III lists the results in detail. Specifically, in NAS-Bench-201 with a sample size of 1000, RBFLex-NAS exhibits superior performance compared to all other state-of-the-art NAS methods, achieving the highest top-1 accuracy of 93.30% over CIFAR-10, 70.99% over CIFAR-100, and 44.57% over ImageNet, respectively. Moreover, our results outperform NASWOT in terms of a smaller variance as Table III shows (i.e., 0.35/0.21/0.70 in RBFLex-NAS vs. 0.84/1.45/2.52 in NASWOT). In NATS-Bench-SSS with a sample size of 1000, our searched top-1 accuracy is 93.16% over CIFAR-10, 70.36% over CIFAR-100, and 46.07% over ImageNet, respectively, higher than the accuracy resulting from all other training-free NAS algorithms. Fig.15 further compares the search cost with respect to network accuracy in NATS-Bench-SSS, showing that RBFLex-NAS can identify networks with higher accuracy yet with less search time in every sample size.

Fig.16 presents the averaged search cost for  $S = 10$  over five runs for various state-of-the-art training-free NAS methods

TABLE III  
COMPARISON ON ARCHITECTURE SEARCH. WEIGHT SHARING METHOD SHARES WEIGHTS TO ALLOW FOR JOINT TRAINING WITH CANDIDATE NETWORKS. IN NAS-BENCH-201, THE TOP-PERFORMING NETWORK FOR EACH DATASET IS IDENTIFIED USING THE CIFAR-10 DATASET. IN NATS-BENCH-SSS, THE TOP-PERFORMING NETWORK FOR EACH DATASET IS DETERMINED USING ITS RESPECTIVE DATASET.

Search Space	Method Metric	Name	CIFAR-10 Accuracy (%)	Search Cost (s)	CIFAR-100 Accuracy (%)	Search Cost (s)	ImageNet Accuracy (%)	Search Cost (s)
NAS Bench 201	Weight Sharing	RSPS	88.10±1.06	1524	66.31±1.29	1524	38.21±2.11	1524
		DARTS(1st)	59.02±13.02	9631	14.99±0.05	9631	16.43±0.79	9631
		DARTS(2nd)	39.77±0.12	28457	15.03±0.07	28457	15.93±0.69	28457
		GDAS	89.14±1.81	4506	70.65±1.51	4506	41.48±3.55	4506
		ENAS	90.17±0.23	2353	70.76±0.69	2353	40.68±0.60	2353
		SETN	88.78±1.10	5886	66.41±1.51	5886	38.96±2.43	5886
	Gradient-based Training-free (requires loss or labels)	ZiCo(S=10)	89.31±1.09	1.28	68.87±1.84	1.28	41.83±3.68	1.28
		ZiCo(S=100)	89.89±0.56	12.82	70.13±1.34	12.82	42.99±3.68	12.82
		ZiCo(S=1000)	90.18±0.25	128.24	70.28±1.12	128.24	43.09±1.95	128.24
		EProxy(S=10)	76.65±10.69	16.12	50.47±12.09	16.12	25.21±8.77	16.12
		EProxy(S=100)	54.70±15.79	179.56	28.57±14.79	179.56	15.53±4.69	179.56
		EProxy(S=1000)	53.51±13.42	1760	27.14±11.83	1760	15.07±1.89	1760
		Synflow(S=10)	86.07±6.18	0.85	62.66±7.55	0.85	34.94±6.18	0.85
		Synflow(S=100)	19.12±25.49	8.81	8.91±21.46	8.81	5.57±3.43	8.81
		Synflow(S=1000)	9.71±1.45	90.65	0.99±2.99	90.65	0.83±6.85	90.65
		grad_norm(S=10)	86.68±5.37	0.78	64.23±6.94	0.78	35.35±7.57	0.78
		grad_norm(S=100)	87.59±1.79	8.12	64.56±3.99	8.12	33.48±7.65	8.12
		grad_norm(S=1000)	86.37±1.66	80.97	61.91±3.45	80.97	27.46±9.25	80.97
		Snip(S=10)	89.27±1.42	8.94	68.71±2.40	8.94	40.98±4.19	8.94
		Snip(S=100)	89.82±1.14	90.13	69.92±2.02	90.13	41.32±4.94	90.13
		Snip(S=1000)	89.70±0.82	912.86	67.69±2.68	912.86	40.59±4.57	912.86
	Layer-based Training-free (no loss and label required)	Random	83.94±12.60	N/A	61.62±11.82	N/A	33.78±8.94	N/A
		NASWOT(S=10)	89.20±1.11	0.64	68.70±1.89	0.64	41.51±3.24	0.64
		NASWOT(S=100)	89.55±0.83	7.15	69.45±1.69	7.15	43.04±2.58	7.15
		NASWOT(S=1000)	89.70±0.84	84.31	69.65±1.45	84.31	43.61±2.52	84.31
		TE-NAS(S=10)	88.28±1.52	10.43	66.39±3.04	10.43	39.02±4.04	10.43
		TE-NAS(S=100)	89.60±0.38	106.38	67.68±0.56	106.38	41.86±1.86	106.38
		TE-NAS(S=1000)	89.76±0.23	1052	67.83±0.55	1052	42.61±1.37	1052
		<b>RBFlEX-NAS(S=10)</b>	<b>93.23±1.29</b>	<b>0.89</b>	<b>70.53±1.70</b>	<b>0.89</b>	<b>41.54±2.65</b>	<b>0.89</b>
		<b>RBFlEX-NAS(S=100)</b>	<b>93.36±0.94</b>	<b>9.17</b>	<b>70.90±0.93</b>	<b>9.17</b>	<b>45.81±0.57</b>	<b>9.17</b>
		<b>RBFlEX-NAS(S=1000)</b>	<b>93.30±0.35</b>	<b>95.36</b>	<b>70.99±0.21</b>	<b>95.36</b>	<b>44.57±0.70</b>	<b>95.36</b>
NATS Bench SSS	Weight Sharing	TAS	93.40±0.00	1946	70.72±0.00	3863	47.17±0.00	7776
		FBNet-v2	93.04±0.18	1377	69.96±0.69	2733	45.05±0.56	5053
		TuNAS	85.84±0.25	1315	57.84±4.19	2672	36.06±0.10	6228
	Gradient-based Training-free (requires loss or labels)	ZiCo(S=10)	89.39±0.50	0.71	67.46±1.83	0.77	42.50±1.83	13.90
		ZiCo(S=100)	89.83±0.32	7.07	68.74±0.97	7.25	44.22±0.96	135.93
		ZiCo(S=1000)	90.03±0.26	69.90	69.36±0.60	69.76	44.90±0.79	1327
		EProxy(S=10)	87.05±1.38	9.94	65.50±2.67	9.10	37.44±4.22	84.39
		EProxy(S=100)	86.55±1.52	96.67	64.16±2.80	95.70	34.59±4.14	842.76
		EProxy(S=1000)	85.76±1.05	988.53	60.74±5.65	990.87	34.80±1.65	8548
		Synflow(S=10)	86.97±1.46	0.39	54.41±5.40	0.39	32.08±4.42	1.43
		Synflow(S=100)	86.13±1.77	3.78	52.07±4.66	3.81	30.74±3.90	12.90
		Synflow(S=1000)	86.96±1.35	37.25	51.24±3.83	37.17	28.85±3.43	126.93
		grad_norm(S=10)	88.34±1.02	0.38	66.05±2.53	0.38	39.95±3.06	4.26
		grad_norm(S=100)	88.52±1.05	3.38	66.75±1.96	3.52	40.23±2.94	41.51
		grad_norm(S=1000)	88.40±1.04	34.42	66.85±1.88	33.07	40.17±2.96	410.43
		Snip(S=10)	89.49±0.45	3.00	68.00±1.33	3.18	42.81±2.02	5.24
		Snip(S=100)	90.04±0.26	60.41	68.97±0.87	62.54	44.65±0.81	83.22
		Snip(S=1000)	90.31±0.11	621.16	69.27±0.79	639.71	45.25±0.32	827.57
	Layer-based Training-free (no loss and label required)	Random	87.90±1.29	N/A	62.43±5.33	N/A	37.13±4.57	N/A
		NASWOT(S=10)	88.95±0.83	0.31	64.42±4.46	0.31	40.61±3.55	1.08
		NASWOT(S=100)	89.73±0.48	2.94	67.12±2.91	2.92	42.94±2.54	11.12
		NASWOT(S=1000)	90.10±0.35	29.53	69.05±1.44	30.62	44.86±0.84	76.26
		TE-NAS(S=10)	88.26±0.95	7.83	61.43±4.77	8.19	37.02±3.75	156.36
		TE-NAS(S=100)	88.52±0.75	76.75	54.39±4.70	78.62	36.48±3.31	1588
		TE-NAS(S=1000)	85.42±2.76	820.74	54.79±4.36	794.64	37.39±1.63	15946
		<b>RBFlEX-NAS(S=10)</b>	<b>92.91±0.33</b>	<b>0.41</b>	<b>69.10±0.89</b>	<b>0.41</b>	<b>45.66±7.10</b>	<b>0.84</b>
		<b>RBFlEX-NAS(S=100)</b>	<b>93.02±0.02</b>	<b>3.95</b>	<b>69.21±1.02</b>	<b>3.96</b>	<b>46.06±0.16</b>	<b>8.17</b>
		<b>RBFlEX-NAS(S=1000)</b>	<b>93.16±0.24</b>	<b>40.51</b>	<b>70.36±0.11</b>	<b>40.15</b>	<b>46.07±0.61</b>	<b>84.03</b>

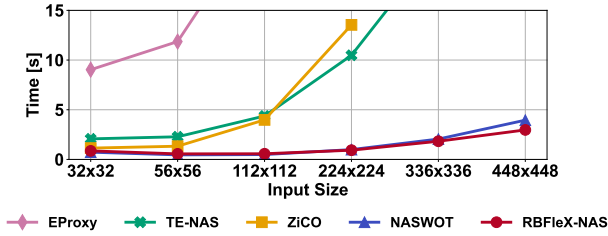


Fig. 16. Comparison of search cost (S=10) vs. input size for different NAS methods. ZiCo is unable to run on inputs larger than  $336 \times 336$  due to insufficient GPU memory (NVIDIA Tesla V100 32GB).

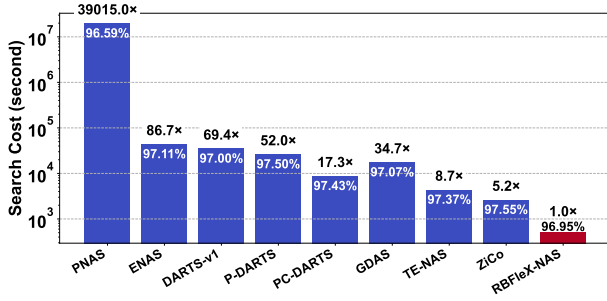


Fig. 17. Comparison of search cost vs. top-1 CIFAR-10 accuracy on DARTS design space. The red dot indicates RBFlex-NAS, running  $5.2 \times$  faster than ZiCo to search the 96.95%-accuracy network.

(i.e., NASWOT, EProxy, TE-NAS, and ZiCo) across different input sizes. Notably, RBFlex-NAS maintains a relatively low and stable search cost as input size increases, outperforming other methods in efficiency. At the largest input size ( $448 \times 448$ ), RBFlex-NAS achieves a search cost of only 2.97 seconds, significantly faster than TE-NAS (39.34 seconds), EProxy (346.2 seconds), and NASWOT (3.95 seconds). Additionally, ZiCo fails to operate with an input size larger than  $336 \times 336$  due to the GPU memory limitation.

Fig.17 compares different NAS methods in the DARTS design space using network accuracy over CIFAR-10 and search cost as metrics. While ZiCo achieves the highest accuracy of 97.55%, RBFlex-NAS closely follows with an accuracy of 96.95%. Notably, ZiCo runs  $5.2 \times$  slower than RBFlex-NAS with only a marginal accuracy improvement of 0.6%.

#### H. Neural Network Activation Function Benchmark (NAFBee) and Evaluation of Non-ReLU Activations

In this experiment, we perform a comparative analysis among our RBFlex-NAS, NASWOT [23], ZiCo [20], TE-NAS [22], grad\_norm [17], snip [18], and synflow [19] on a design space with activation functions. To accomplish this, we have created the Neural Network Activation Function Benchmark (NAFBee). NAFBee utilizes VGG-19 and BERT<sub>BASE</sub> [2] network as backbones. We replace all activation functions on a backbone with various types of activation functions and build architecture candidates. We select widely used activation functions such as ReLU, GELU [60], SiLU [61], LeakyReLU, ReLU6, Mish [62], Hardswish, CELU [63], ELU [64], Hardtanh, and SELU [65]. Therefore, NAFBee (VGG-19) and NAFBee (BERT) each have 11 architecture candidates.

We then acquire the ground-truth accuracy of each candidate network in NAFBee (VGG-19) and NAFBee (BERT) via training. For NAFBee (VGG-19), the 200-epoch training deploys the SGD optimizer with a cosine decay learning rate from 0.1 to 0, a momentum of 0.9, a weight decay of  $5e-4$  and a batch size of 128. This configuration is inspired by NATS-Bench [27]. The target dataset to work with NAFBee (VGG-19) is CIFAR-10 which has been preprocessed by randomly cropping to  $32 \times 32$  pixels with 4-pixel padding on each border as well as horizontal random flipping and normalizing across the RGB channels. For NAFBee (BERT), we utilize the same fine-tuning parameters as in the BERT paper [2]. The target dataset for demonstration is Stanford Sentiment Treebank (SST-2) [66]. SST-2 incorporates a total of 215,154 unique phrases for binary classification. RBFlex-NAS and the training-free NAS algorithms under comparison evaluate each network configuration with the aforementioned activation functions. In the evaluation phase, we compute the correlation coefficients between the ground-truth accuracy and the corresponding scores over CIFAR-10 using VGG-19 and over SST-2 using BERT. The batch size  $N$  for RBFlex-NAS and NASWOT is 16. The number of networks  $M$  for HDA is 1.

Table IV shows the experimental results obtained using NAFBee (VGG-19). The ReLU activation function achieves the highest performance with an accuracy of 91.06%. RBFlex-NAS successfully identifies this optimal network configuration with the highest score, whereas other training-free NAS fail to achieve it.

Table V shows the scores and correlation values by different training-free proxies using NAFBee (BERT). The BERT model with GELU activation function achieves the highest accuracy of 92.97%. RBFlex-NAS outperforms both layer-based and gradient-based NAS as it successfully identifies the best-performing network during activation function search. In addition, the Kendall correlation of RBFlex-NAS when scoring the network with GELU is 0.443 while the correlation of TE-NAS is merely 0.058. Apparently, RBFlex-NAS can accurately evaluate networks incorporating various widely adopted activation functions, expanding the design space with activation function exploration for network architecture search.

#### V. CONCLUSION

This work introduces RBFlex-NAS, a training-free NAS approach that leverages a Radial Basis Function (RBF) kernel with a hyperparameter detection algorithm. RBFlex-NAS evaluates candidate networks based on the similarity of activation outputs and input feature maps from the last layer of a network across different input images. It demonstrates superior top-1 accuracy in network search and excellent Kendall correlation across diverse design spaces in image classification, object classification/segmentation, and natural language processing tasks.

Additionally, we present NAFBee, a novel benchmarking design space that supports a broader range of activation functions, enabling activation function exploration. Compared to state-of-the-art training-free NAS methods, RBFlex-NAS



TABLE IV  
THE SCORE RESULT IN NAFBEE(VGG-19). PEARSON AND KENDALL CORRELATION BETWEEN VALIDATED ACCURACY AND SCORE.

Design Space	Activation Functions	Accuracy(%)	Score						
			Layer-based			Gradient-based			
			<b>RBFlE</b> X-NAS	NASWOT	TE-NAS	grad_norm	snip	synflow	ZiCo
NAFBee (VGG-19)	ReLU	<b>91.06</b>	<b>-6190.45</b>	191.72	-2.11	573.13	3569.66	5.19E+22	259.02
	GELU [60]	91.03	-6207.12	<b>192.04</b>	-4.45	478.64	3045.44	5.25E+22	257.28
	SiLU [61]	91.03	-6212.32	191.88	-9.33	329.59	2027.23	5.01E+22	257.98
	LeakyReLU	90.75	-6195.74	191.75	-2.10	560.38	3547.21	5.19E+22	257.89
	ReLU6	90.61	-6194.21	191.62	-2.14	<b>574.87</b>	<b>3574.24</b>	6.79E+02	<b>259.98</b>
	Mish [62]	90.54	-6202.14	192.00	-2.43	426.65	2810.60	5.19E+22	258.78
	Hardswish	89.94	-6224.58	191.80	-181.95	473.98	2830.19	4.85E+22	257.09
	CELU [63]	88.36	-6216.53	191.95	-1.62	302.95	2126.31	5.42E+22	257.35
	ELU [64]	87.01	-6215.80	191.84	<b>-1.61</b>	313.30	2182.29	5.17E+22	259.02
	Hardtanh	86.74	-6216.71	192.00	-2.08	566.95	3501.04	114.17	258.33
	SELU [65]	85.83	-6217.89	191.97	-1.64	345.97	2404.90	<b>1.12E+23</b>	259.57
Pearson Correlation			0.623	-0.384	-0.117	0.708	-0.417	-0.574	-0.255
Kendall Correlation			0.550	-0.240	-0.367	0.257	0.220	0.019	-0.110

TABLE V  
THE SCORE RESULT IN NAFBEE(BERT). PEARSON AND KENDALL CORRELATION BETWEEN VALIDATED ACCURACY AND SCORE.

Design Space	Activation Functions	Accuracy(%)	Score						
			Layer-based			Gradient-based			
			<b>RBFlE</b> X-NAS	NASWOT	TE-NAS	grad_norm	snip	synflow	ZiCo
NAFBee (BERT)	GELU	<b>92.97</b>	<b>-4388.62</b>	198.05	<b>-16.09</b>	194.23	2441.72	5.07e-13	1193
	ReLU	92.26	-5635.96	174.57	-159.27	36.45	193.71	2.68e-13	1161
	LeakyReLU	91.76	-5406.85	181.83	-133.37	50.05	589.93	2.36e-13	<b>1231</b>
	ReLU6	91.60	-5664.52	173.18	-173.63	17.18	155.81	1.09e-12	1188
	SiLU	86.77	-4516.79	200.1	-44.06	238.28	<b>8276.62</b>	8.77e-13	1198
	Hardswish	85.23	-4460.36	<b>203.95</b>	-34.41	418.03	4980.75	8.51e-13	1200
	Mish	84.51	-4437.43	201.51	-28.62	<b>547.23</b>	4268.57	8.81e-13	1183
	ELU	49.92	-7638.97	176.97	-110.74	2.73	144.42	8.06e-13	1193
	Hardtanh	49.92	-7621.49	176.72	-120.74	22.66	10.89	4.37e-13	1168
	SELU	49.92	-7482.86	173.16	-147.15	11.81	24.95	1.02e-12	1169
	CELU	49.92	-7637.44	177.17	-134.80	10.05	58.23	<b>1.82e-12</b>	1176
Pearson Correlation			0.906	0.484	0.306	0.433	0.436	-0.434	0.425
Kendall Correlation			0.443	0.135	0.058	0.289	0.443	-0.289	0.250

accurately identifies the best-performing networks with activation function searches for architectures such as VGG-19 and BERT. Furthermore, it offers rapid network evaluation, requiring only seconds to assess a candidate network. This makes it a highly efficient tool for identifying optimal architectures for diverse AI applications.

## REFERENCES

- [1] K. C. Nanda, E. N. Computer, S. K. Ch., and C. B. Madhavi, "Real-time face mask detection using computer vision and machine learning," in *Proceedings of the 2023 Second International Conference on Electronics and Renewable Systems*, pp. 1532–1537, 2023.
- [2] D. Jacob, C. Ming-Wei, L. Kenton, and T. Kristina, "BERT: Pre-training of deep bidirectional transformers for language understanding," in *Proceedings of the 2019 Conference of the North American Chapter of the Association for Computational Linguistics: Human Language Technologies*, vol. 1, pp. 4171–4186, 2019.
- [3] F. Wenqi, M. Yao, L. Qing, H. Yuan, Z. Eric, T. Jiliang, and Y. Dawei, "Graph neural networks for social recommendation," in *Proceeding of the 2019 World Wide Web Conference*, p. 417–426, 2019.
- [4] L. Michael, Y. Yavuz, O. Ozgur, Z. Zhuoran, T. Shin-Yeh, W. Carole-Jean, and H. Mark, "Understanding capacity-driven scale-out neural recommendation inference," in *Proceeding of the 2021 IEEE International Symposium on Performance Analysis of Systems and Software*, pp. 162–171, 2021.
- [5] B. Zoph and Q. Le, "Neural architecture search with reinforcement learning," in *Proceeding of the 5th International Conference on Learning Representations*, 2017.
- [6] Z. Barret, V. Vijay, S. Jonathon, and L. Q. V, "Learning transferable architectures for scalable image recognition," in *Proceeding of the 2018 IEEE/CVF Conference on Computer Vision and Pattern Recognition*, pp. 8697–8710, 2018.
- [7] P. Hieu, G. Melody, Z. Barret, L. Quoc, and D. Jeff, "Efficient neural architecture search via parameters sharing," in *Proceedings of the 35th International Conference on Machine Learning*, vol. 80, pp. 4095–4104, 2018.
- [8] L. Xiangzhong, L. Di, H. Shuo, K. Hao, C. Hui, and L. Weichen, "Designing efficient dnns via hardware-aware neural architecture search and beyond," *IEEE Transactions on Computer-Aided Design of Integrated Circuits and Systems*, vol. 41, no. 6, pp. 1799–1812, 2022.
- [9] J. Weiwen, Y. Lei, S. E. Hsing-Mean, Z. Qingfeng, G. Shouzheng, D. Sakyasingha, S. Yiyu, and H. Jingtong, "Hardware/software co-exploration of neural architectures," *IEEE Transactions on Computer-Aided Design of Integrated Circuits and Systems*, vol. 39, no. 12, pp. 4805–4815, 2020.
- [10] W. Lanfei, X. Lingxi, B. Kaifeng, Z. Kaili, G. Jun, and T. Qi, "M<sup>2</sup>nas: Joint neural architecture optimization system with network transmission," *IEEE Transactions on Computer-Aided Design of Integrated Circuits and Systems*, vol. 42, no. 8, pp. 2631–2642, 2023.
- [11] L. Jaeseong, R. Jungsub, K. Duseok, and H. Soonhoi, "Snas: Fast hardware-aware neural architecture search methodology," *IEEE Transactions on Computer-Aided Design of Integrated Circuits and Systems*, vol. 41, no. 11, pp. 4826–4836, 2022.
- [12] J. Weiwen, Y. Lei, D. Sakyasingha, H. Jingtong, and S. Yiyu, "Standing on the shoulders of giants: Hardware and neural architecture co-search with hot start," *IEEE Transactions on Computer-Aided Design of Integrated Circuits and Systems*, vol. 39, no. 11, pp. 4154–4165, 2020.
- [13] L. Xiangzhong, L. Di, K. Hao, H. Shuo, C. Hui, and L. Weichen, "Lightnas: On lightweight and scalable neural architecture search for embedded platforms," *IEEE Transactions on Computer-Aided Design of Integrated Circuits and Systems*, vol. 42, no. 6, pp. 1784–1797, 2023.

- [14] S. Yanan, W. Handing, X. Bing, J. Yaochu, G. Y. Gary, and Z. Mengjie, "Surrogate-assisted evolutionary deep learning using an end-to-end random forest-based performance predictor," *IEEE Transactions on Evolutionary Computation*, vol. 24, no. 2, pp. 350–364, 2020.
- [15] Y. Tang, Y. Wang, Y. Xu, H. Chen, B. Shi, C. Xu, C. Xu, Q. Tian, and C. Xu, "A semi-supervised assessor of neural architectures," in *proceeding of the 2020 IEEE/CVF Conference on Computer Vision and Pattern Recognition*, pp. 1807–1816, 2020.
- [16] H. Shayan, D. Xiaoliang, and K. J. Niraj, "Curious: Efficient neural architecture search based on a performance predictor and evolutionary search," *IEEE Transactions on Computer-Aided Design of Integrated Circuits and Systems*, vol. 41, no. 11, pp. 4975–4990, 2022.
- [17] M. S. Abdelfattah, A. Mehrotra, Ł. Dudziak, and N. D. Lane, "Zero-Cost Proxies for Lightweight NAS," in *Proceeding of the 9th International Conference on Learning Representations*, 2021.
- [18] L. Namhoon, A. Thalaiyasingam, and T. P. HS, "Snip: Single-shot network pruning based on connection sensitivity," in *Proceeding of the 7th International Conference on Learning Representations*, 2019.
- [19] T. Hidenori, K. Daniel, Y. D. L., and G. Surya, "Pruning neural networks without any data by iteratively conserving synaptic flow," in *Advances in Neural Information Processing Systems*, vol. 33, pp. 6377–6389, 2020.
- [20] G. Li, Y. Yang, K. Bhardwaj, and R. Marculescu, "Zico: Zero-shot NAS via inverse coefficient of variation on gradients," in *The Eleventh International Conference on Learning Representations*, 2023.
- [21] Y. Li, J. Li, C. Hao, P. Li, J. Xiong, and D. Chen, "Extensible and efficient proxy for neural architecture search," in *Proceedings of the IEEE/CVF International Conference on Computer Vision*, pp. 6199–6210, 2023.
- [22] W. Chen, X. Gong, and Z. Wang, "Neural architecture search on imagenet in four gpu hours: A theoretically inspired perspective," in *International Conference on Learning Representations (ICLR)*, 2021.
- [23] J. Mellor, J. Turner, A. Storkey, and E. J. Crowley, "Neural architecture search without training," in *Proceeding of the 20th International Conference on Machine Learning*, 2021.
- [24] Y. Liu, H. Li, Y. Sun, and S. Liu, "Das: Neural architecture search via distinguishing activation score," *ArXiv*, vol. abs/2212.12132, 2022.
- [25] Y. Jason, C. Jeff, B. Yoshua, and L. Hod, "How transferable are features in deep neural networks?," *Advances in neural information processing systems*, vol. 27, 2014.
- [26] D. Xuanyi and Y. Yi, "Nas-bench-201: Extending the scope of reproducible neural architecture search," in *Proceeding of the 8th International Conference on Learning Representations*, 2020.
- [27] D. Xuanyi, L. Lu, M. Katarzyna, and G. Bogdan, "Nats-bench: Benchmarking nas algorithms for architecture topology and size," *IEEE transactions on pattern analysis and machine intelligence*, vol. 44, no. 7, pp. 3634–3646, 2021.
- [28] R. Ilija, J. Justin, X. Saining, L. Wan-Yen, and D. Piotr, "On network design spaces for visual recognition," in *Proceeding of the 2019 IEEE/CVF International Conference on Computer Vision*, 2019.
- [29] Y. Duan, X. Chen, H. Xu, Z. Chen, X. Liang, T. Zhang, and Z. Li, "Transnas-bench-101: Improving transferability and generalizability of cross-task neural architecture search," in *Proceedings of the IEEE/CVF Conference on Computer Vision and Pattern Recognition*, pp. 5251–5260, 2021.
- [30] R. Esteban, A. Alok, H. Yanping, and V. L. Quoc, "Regularized evolution for image classifier architecture search," in *Proceedings of the Thirty-Third AAAI Conference on Artificial Intelligence and Thirty-First Innovative Applications of Artificial Intelligence Conference and Ninth AAAI Symposium on Educational Advances in Artificial Intelligence*, 2019.
- [31] L. Hanxiao, S. Karen, and Y. Yiming, "Darts: Differentiable architecture search," in *Proceeding of the 7th International Conference on Learning Representations*, 2019.
- [32] Q. Yijian, W. Xin, C. Peng, and Z. Wenwu, "Gqnas: Graph q network for neural architecture search," in *Proceeding of the 2021 IEEE International Conference on Data Mining*, pp. 1288–1293, 2021.
- [33] B. Jianrong, N. Jianyuan, L. Chao, J. Bin, Z. Fang, and H. Jianhai, "Improved blind spectrum sensing by covariance matrix cholesky decomposition and rbf-svm decision classification at low snrs," *IEEE Access*, vol. 7, pp. 97117–97129, 2019.
- [34] K. Bor-Chen, H. Hsin-Hua, L. Cheng-Hsuan, H. Chih-Cheng, and T. Jin-Shiuh, "A kernel-based feature selection method for svm with rbf kernel for hyperspectral image classification," *IEEE Journal of Selected Topics in Applied Earth Observations and Remote Sensing*, vol. 7, no. 1, pp. 317–326, 2014.
- [35] G.-B. Huang, P. Saratchandran, and N. Sundararajan, "An efficient sequential learning algorithm for growing and pruning rbf (gap-rbf) networks," *IEEE Transactions on Systems, Man, and Cybernetics, Part B (Cybernetics)*, vol. 34, no. 6, pp. 2284–2292, 2004.
- [36] H. Kohei, T. Takashi, T. Ryota, and K. Hisashi, "Self-measuring similarity for multi-task gaussian process," in *Proceedings of ICML Workshop on Unsupervised and Transfer Learning*, vol. 27, pp. 145–153, 2012.
- [37] V. Jean-Philippe, T. Koji, and S. Bernhard, "A primer on kernel methods," *Kernel methods in computational biology*, vol. 47, pp. 35–70, 2004.
- [38] V. A. Alfred and E. H. John, *The design and analysis of computer algorithms*. Pearson Education India, 1974.
- [39] G. C. Valls, L. G. Chova, J. C. Maravilla, J. M. Guerrero, E. S. Olivas, L. A. Chorda, and J. Moreno, "Robust support vector method for hyperspectral data classification and knowledge discovery," *IEEE Transactions on Geoscience and Remote Sensing*, vol. 42, no. 7, pp. 1530–1542, 2004.
- [40] W. Wang, Z. Xu, W. Lu, and X. Zhang, "Determination of the spread parameter in the gaussian kernel for classification and regression," *Neurocomputing*, vol. 55, no. 3, pp. 643–663, 2003.
- [41] F. Keinosuke, *Introduction to statistical pattern recognition*. Elsevier, 2013.
- [42] A. R. Zamir, A. Sax, W. Shen, L. J. Guibas, J. Malik, and S. Savarese, "Taskonomy: Disentangling task transfer learning," in *Proceedings of the IEEE conference on computer vision and pattern recognition*, pp. 3712–3722, 2018.
- [43] K. He, X. Zhang, S. Ren, and J. Sun, "Delving deep into rectifiers: Surpassing human-level performance on imagenet classification," in *Proceeding of 2015 IEEE International Conference on Computer Vision*, pp. 1026–1034, 2015.
- [44] K. Simonyan and A. Zisserman, "Very deep convolutional networks for large-scale image recognition," in *Proceeding of the 3rd International Conference on Learning Representations*, pp. 1–14, 2015.
- [45] K. S. Yuan, *Kernel methods and machine learning*. Cambridge University Press, 2014.
- [46] H. Alain and Z. Djemel, "Image quality metrics: Psnr vs. ssim," in *Proceeding of the 20th International Conference on Pattern Recognition*, pp. 2366–2369, 2010.
- [47] Z. Wang, A. Bovik, H. Sheikh, and E. Simoncelli, "Image quality assessment: from error visibility to structural similarity," *IEEE Transactions on Image Processing*, vol. 13, no. 4, pp. 600–612, 2004.
- [48] C. Israel, H. Yiteng, C. Jingdong, B. Jacob, B. Jacob, C. Jingdong, H. Yiteng, and C. Israel, "Pearson correlation coefficient," *Noise reduction in speech processing*, pp. 1–4, 2009.
- [49] B. Jens, M. Jana, and D. Riehle, "Effect of transparency and trust on acceptance of automatic online comment moderation systems," in *2019 IEEE 21st Conference on Business Informatics (CBI)*, vol. 01, pp. 429–435, 2019.
- [50] Y. Kurihara, T. Yamasaki, T. Kaburagi, S. Kumagai, and T. Matsumoto, "Model of urine accumulation in the bladder and method for predicting unconstrained urine volume based on absorption spectrum of urine," *IEEE Access*, vol. 8, pp. 69368–69377, 2020.
- [51] L. Liam and T. Ameet, "Random search and reproducibility for neural architecture search," in *Proceedings of The 35th Uncertainty in Artificial Intelligence Conference*, pp. 367–377, 2020.
- [52] D. Xuanyi and Y. Yi, "Searching for a robust neural architecture in four gpu hours," in *Proceedings of the IEEE/CVF Conference on Computer Vision and Pattern Recognition*, pp. 1761–1770, 2019.
- [53] Dong Xuanyi and Yang Yi, "One-shot neural architecture search via self-evaluated template network," in *Proceeding of the IEEE/CVF International Conference on Computer Vision*, pp. 3680–3689, 2019.
- [54] D. Xuanyi and Y. Yi, "Network pruning via transformable architecture search," in *Proceeding of the 33rd Conference on Neural Information Processing Systems*, 2019.
- [55] A. Wan, X. Dai, P. Zhang, Z. He, Y. Tian, S. Xie, B. Wu, M. Yu, T. Xu, K. Chen, P. Vajda, and J. E. Gonzalez, "Fbnetv2: Differentiable neural architecture search for spatial and channel dimensions," in *Proceeding of the IEEE/CVF Conference on Computer Vision and Pattern Recognition*, pp. 12962–12971, 2020.
- [56] G. Bender, H. Liu, B. Chen, G. Chu, S. Cheng, P.-J. Kindermans, and Q. V. Le, "Can weight sharing outperform random architecture search? an investigation with tunas," in *Proceedings of the IEEE/CVF conference on computer vision and pattern recognition*, pp. 14323–14332, 2020.
- [57] X. Chen, L. Xie, J. Wu, and Q. Tian, "Progressive differentiable architecture search: Bridging the depth gap between search and evaluation," in *Proceedings of the IEEE/CVF international conference on computer vision*, pp. 1294–1303, 2019.
- [58] Y. Xu, L. Xie, X. Zhang, X. Chen, G.-J. Qi, Q. Tian, and H. Xiong, "Pc-darts: Partial channel connections for memory-efficient architecture search," in *International Conference on Learning Representations*, 2020.

- [59] C. Liu, B. Zoph, M. Neumann, J. Shlens, W. Hua, L.-J. Li, L. Fei-Fei, A. Yuille, J. Huang, and K. Murphy, "Progressive neural architecture search," in *Proceedings of the European conference on computer vision (ECCV)*, pp. 19–34, 2018.
- [60] H. Dan and G. Kevin, "Bridging nonlinearities and stochastic regularizers with gaussian error linear units," in *Proceeding of the 5th International Conference on Learning Representations*, 2017.
- [61] S. Elfving, E. Uchibe, and K. Doya, "Sigmoid-weighted linear units for neural network function approximation in reinforcement learning," *Neural Networks*, vol. 107, pp. 3–11, 2018.
- [62] M. Diganta, "Mish: A self regularized non-monotonic activation function," in *Proceeding of the 31th British Machine Vision Conference*, 2020.
- [63] J. T. Barron, "Continuously differentiable exponential linear units," *arXiv preprint arXiv:1704.07483*, 2017.
- [64] D. A. Clevert, T. Unterthiner, and S. Hochreiter, "Fast and accurate deep network learning by exponential linear units (elus)," in *Proceeding of the 4th International Conference on Learning Representations*, 2016.
- [65] K. Günter, U. Thomas, M. Andreas, and H. Sepp, "Self-normalizing neural networks," *Advances in neural information processing systems*, vol. 30, 2017.
- [66] R. Socher, A. Perelygin, J. C. Jean Wu, C. Manning, A. Ng, and C. Potts, "Recursive deep models for semantic compositionality over a sentiment treebank," in *Proceedings of the 2013 Conference on Empirical Methods in Natural Language Processing*, p. 1631–1642, 2013.



**Tomomasa Yamasaki** received his B.Eng. and M.Eng. degrees in System Engineering from Aoyama Gakuin University, Tokyo, Japan. He is currently pursuing a Ph.D. in Computer Science at the Singapore University of Technology and Design (SUTD), Singapore. His research interests focus on neural architecture search (NAS), and design automation tools for hardware–software co-optimization.

He received the Best Paper Award at the ACM/IEEE International Symposium on Low Power Electronics and Design (ISLPED) in 2023. He was also a recipient of the Best Student Paper Award at the 8th IIAE International Conference on Industrial Application Engineering in 2020.

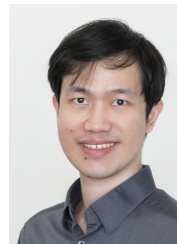


**Zhehui Wang** received B.S. degree in Electrical Engineering from Fudan University, China, in 2010, and Ph.D. degree in Electronic and Computer Engineering from Hong Kong University of Science and Technology, Hong Kong, in 2016. He is currently a Research Scientist with the Institute of High Performance Computing, Agency for Science, Technology and Research, Singapore. He authored and co-authored more than 60 research papers in peer-reviewed journals, conferences, and books. His research interests include efficient AI

deployment, AI on emerging technologies, hardware–software co-design, and high-performance computing.



**Luo Tao** received his bachelor's degree from the Harbin Institute of Technology, Harbin, China, in 2010, his master's degree from the University of Electronic Science and Technology of China, Chengdu, China, in 2013, and his Ph.D. degree from the School of Computer Science and Engineering, Nanyang Technological University, Singapore, in 2018. He is currently a senior research scientist with the Institute of High Performance Computing (IHPC), Agency for Science, Technology and Research, Singapore (A\*STAR), Singapore. His current research interests include high-performance computing, machine learning, computer architecture, hardware–software co-exploration, quantum computing, efficient AI and its application.



**Niangjun Chen** received the B.S. degree in Computer Science from the University of Cambridge and the M.S. and Ph.D. degrees in Computer Science from the California Institute of Technology. After graduating in 2017, he joined the Institute of High Performance Computing as a Research Scientist working on optimizing logistics and modeling and simulation of the transport systems. Since September 2020, he has been an Assistant Professor with the Singapore University of Technology and Design. He has a joint appointment with the Institute for High

Performance Computing, Agency for Science, Technology, and Research. His research interests include optimization, machine learning, game theory, and their applications to complex systems such as smart grids, data centers, and transport.



**Bo Wang** received the Ph.D. degree in Electrical and Electronic Engineering from Nanyang Technological University, Singapore, in 2015. From 2015 to 2016, she worked as a Staff Circuit Design Engineer at MediaTek, Singapore. She then joined the National University of Singapore as a Post-Doctoral Research Fellow from 2016 to 2020. Since 2020, she has been an Assistant Professor at the Singapore University of Technology and Design, Singapore. She has authored and co-authored many papers published in prestigious journals and conference proceedings,

including JSSC, TCAS-I, TVLSI, TCAS-II, A-SSCC, DAC, DATE, ISLPED, and MobiSys. Her research interests span various aspects of energy-efficient system, architecture and circuit design, as well as design automation tools for hardware–software co-optimization.

Dr. Wang received the Distinguished Design Award at the IEEE Asian Solid-State Circuits Conference (A-SSCC) in 2023. She was also a recipient of the Best Paper Award at the ACM/IEEE International Symposium on Low Power Electronics and Design (ISLPED) in 2023 and the International SoC Design Conference (ISOCC) in 2024 and 2014. She currently serves as an Associate Editor for the IEEE Open Journal of Circuits and Systems and has served as a Guest Editor for Frontiers in Neuroscience.